Fractal Growth Phenomena

Tamás Vicsek

Institute for Technical Physics
Budapest, Hungary

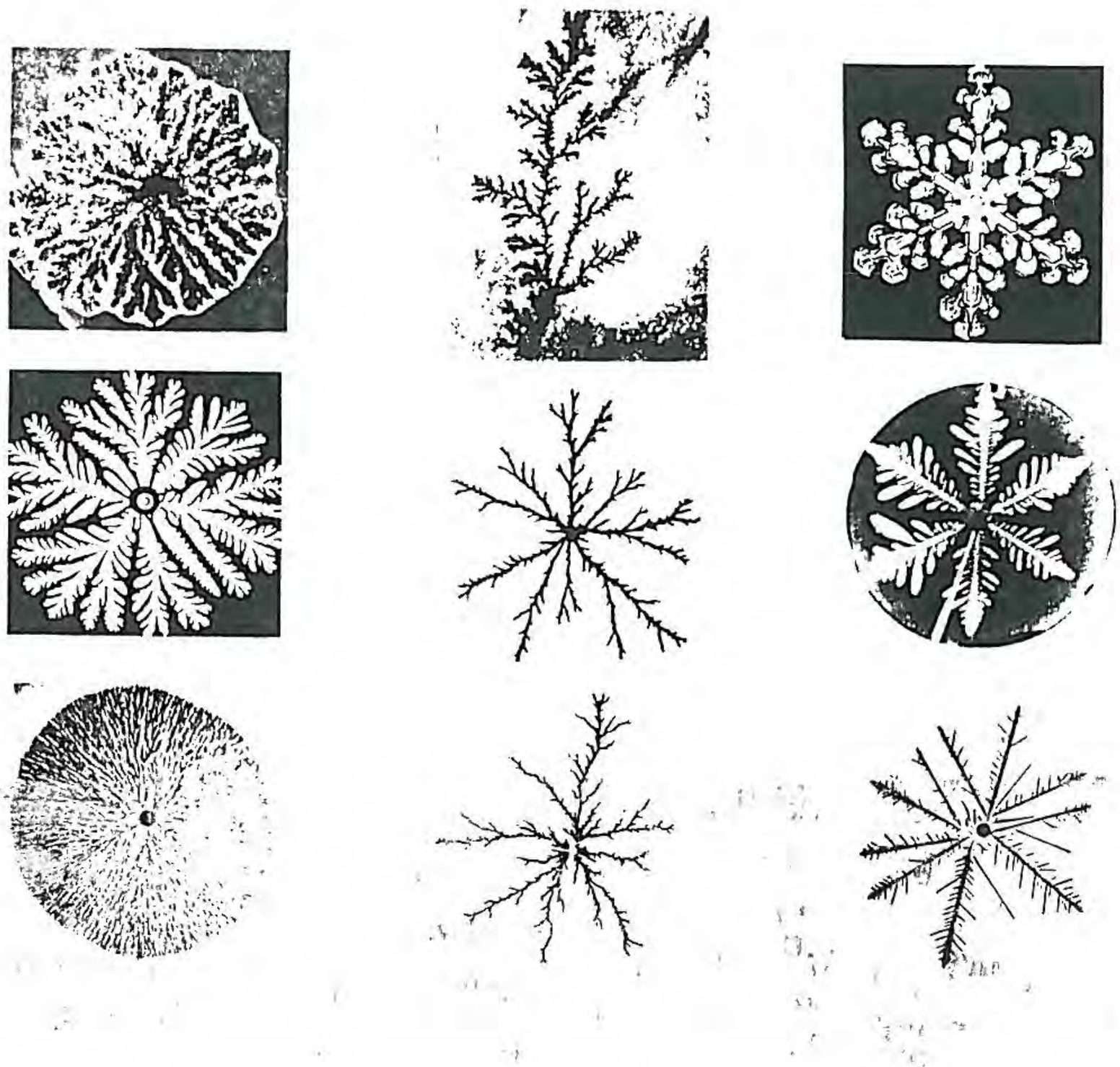

WORLD SCIENTIFIC
Singapore

$D = A \cdot b^{\alpha}$

$C(r) \sim A r^{\alpha} \quad r \to br \quad C(br) \sim D r^{\alpha}$

Scaling, new-analitikus, kritikus viselkedés, kritikus pont univerzális

kritikus exponensek

Part III

FRACTAL PATTERN FORMATION

Chapter 9.

COMPUTER SIMULATIONS

The formation of complex patterns by moving unstable interfaces is a common phenomenon in many fields of science and technology. During *pattern formation* in real systems the *surface tension* of the boundary between the growing and the surrounding phases plays an important role. This is in contrast to the case of cluster growth models discussed in Part II., where such effects were not taken into account. Thus we shall use the term pattern formation for growth processes in which surface tension is essential.

As will be discussed in the present Part, in addition to surface tension and its *anisotropy*, such further parameters as the amount of *fluctuations* and the *driving force* can influence the geometry of the resulting interfacial patterns. Depending on the values of these parameters a great variety of patterns are found experimentally (see Fig. 1.1). In many cases the morphology of the growing phase is very complex and can be described in terms of fractal geometry.

We shall be concerned with systems in which the motion of the phase boundary is controlled by a field-like quantity which satisfies the Laplace equation. The most typical examples for diffusion-limited or Laplacian growth include solidification, when a crystalline phase is growing in an undercooled melt, the development of viscous fingers which can be observed when a less viscous fluid is injected into a more viscous one, and electrodeposition,

where the ions diffusing in an electrolite give rise to beautiful patterns being deposited onto the cathode.

There are three major approaches which can be used to investigate the structure and development of Laplacian patterns:
i) *Stability analysis* of the original equations and their simplified versions allow one to study such questions as the selected velocity and the tip radius of an advancing dendrite or finger. The crucial role of the surface tension and its anisotropy was first pointed out in these investigations. Those who are interested in the theoretical aspects of pattern formation can find excellent treatment of the problem in a number of recent review articles (Langer 1980, Bensimon *et al* 1986, Kessler *et al* 1987, 1988). Here we shall concentrate on the next two approaches.
ii) If one is interested in the description of complex geometrical patterns, it is effective to use such numerical methods as *computer simulations* of aggregation models or other, more standard algorithms. These will be discussed in the present Chapter.
iii) *Experiments* on Laplacian growth represent the third approach to the study of interfacial pattern formation. Such investigations are usually inexpensive and in many cases they can be carried out without great efforts. During the past few years the related experiments (to be reviewed in Chapter 10.) have made an important contribution to our understanding of diffusion-limited growth.

9.1. EQUATIONS

As discussed above, under certain approximations the same equations can be used for the description of a wide range of pattern forming phenomena. We shall write these equations for the dimensionless field-like variable $u(\vec{x},t)$, which may denote temperature (solidification), pressure (viscous fingering) electric potential (electrodeposition, dielectric breakdown) or concentration (isothermal solidification, electrodeposition) (Langer 1980, Bensimon *et al* 1986, Kessler *et al* 1987, 1988). In various approximations the interface in diffusion-limited processes is determined by the Laplace equation

$$\nabla^2 u(\vec{x}, t) = 0 \tag{9.1}$$

with appropriate boundary conditions. For example, for solidification equation (9.1) follows from the approximation that the velocity of the interface is small compared with the characteristic time needed for u to relax to a stationary distribution corresponding to the given shape of the changing interface (then the left hand side of the diffusion equation $\partial u/\partial t = C\nabla^2 u$, which expresses heat conservation, can be neglected). In the case of viscous fingering in a porous medium or in two dimensions, (9.1) corresponds to the assumption of incompressibility of the fluids. Obviously, the distribution of the electric potential in electrodeposition experiments also satisfies (9.1) in regions where there are no sources of charge present.

The normal velocity of the interface is given by the first boundary condition

$$v_n = -c\hat{\mathbf{n}} \cdot \nabla u, \tag{9.2}$$

where c is a constant and $\hat{\mathbf{n}}$ denotes the unit vector normal to the interface. Thus the local interfacial velocity is proportional to the gradient of the field. As an example, one can mention solidification, where (9.2) is a consequence of heat conservation: the latent heat produced at the interface (which is proportional to v_n) should be equal to the heat flux away from the surface (which is proportional to the temperature gradient). In (9.2) it is assumed that $\nabla u = 0$ in the growing phase.

The growth is induced by the fact that the value of the field far from the interface is a constant

$$u_\infty = Const. \tag{9.3}$$

different from the equilibrium value of u at the interface Γ. If one uses the dimensionless form of the equations, this equilibrium value is equal to zero. Thus, unstable growth (negative gradient at the interface) takes place

for $u_\infty < 0$. In the following we shall assume this. Finally, the boundary condition given below prescribes u on the growing interface

$$u_\Gamma = -d_0\kappa - \beta v_n^\eta, \tag{9.4}$$

where the so called capillary length d_0 is proportional to the surface tension, κ denotes the local curvature of the interface (with $\kappa > 0$ for a sphere), β is the kinetic coefficient and η is an exponent depending on the physical process considered. The local curvature can be calculated using the expression $\kappa = 1/R_1 + ... + 1/R_{d-1}$, where R_i are the local principal radii of curvature of the surface.

A few additional remarks may be useful in explaining the form of the boundary condition (9.4).

i) It is clear from (9.4) that u is made dimensionless in such a way that $u = 0$ for a resting planar interface.

ii) With $\beta = 0$, (9.4) reduces to the *Gibbs-Thomson* relation which is valid assuming local thermodynamic equilibrium. It can be understood on a qualitativel basis. Let us use the language of solidification problems. At equilibrium the same number of particles are leaving the solid as are becoming part of it. If the surface has a part with positive curvature (bump), the situation changes since the molecules in this region can leave the surface easier (because the molecules on the surface have fewer neighbours with attractive interactions bonding them to the growing phase). Assume that the sample is at a temperature (melting temperature) at which the planar interface is in equilibrium. Then a bump will melt back which is equivalent to the statement that the melting temperature at the bump is decreased. For places with negative curvature the situation is reversed. This is expressed by the first term of the right-hand side of (9.4).

iii) The *kinetic coefficient* β has various origins depending on the given growth process (see e.g. Park and Homsy (1985) for viscous fingering), but in each case it reflects the fact that the moving interface represents a departure from equilibrium.

Although the Laplace equation is linear, because of the above bound-

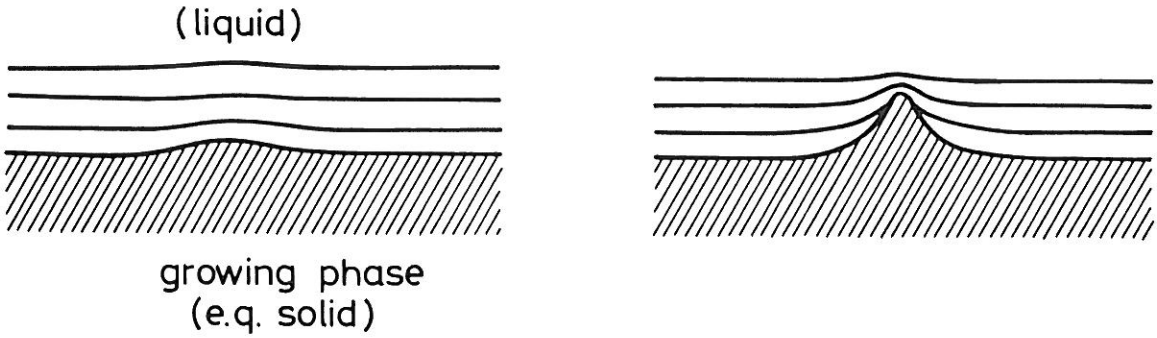

Figure 9.1. Schematic illustration of the Mullins-Sekerka instability. The function u (e.g. the temperature) is the same along the lines drawn close to the interface.

ary conditions the mathematical problem posed by (9.1-9.4) is *non-linear* and except for a few simple cases it can not be solved analytically. This non-linearity is manifested in the *Mullins-Sekerka instability* (Mullins and Sekerka 1963) which takes place whenever one part of the interface advances locally faster than the surrounding region. The gradient of the field around a protrusion becomes larger in analogy with the electric field which is known to become very large close to the tip of a charged needle (see Fig 9.1). The increased gradient leads to a faster growth of the interface (because of (9.2)) which, in turn, results in a further increase of the gradient.

Due to the instability small protruding perturbations of the interface grow exponentially. For short wavelengths, however, the surface tension stabilizes the interface and this mechanism introduces a characteristic length (Mullins and Sekerka 1963). This can be shown by linearizing the diferential equation and boundary conditions (9.2) and (9.4) in a perturbation about the steady state solution corresponding to a planar interface moving with a constant velocity v. Assuming that the perturbation has the form $\delta(x,t) = \delta_0 e^{\omega t + ikx}$ with $\delta_0 \ll 1$ the following expression can be obtained for the *dispersion relation*

$$\omega(k) \simeq kv(1 - ld_0k^2), \tag{9.5}$$

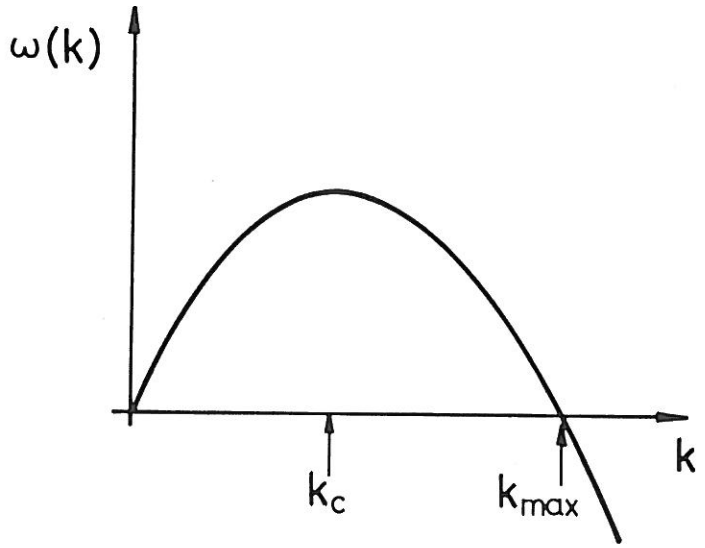

Figure 9.2. Schematic representation of the dispersion relation (9.5). Deformations with a characteristic wave number k for which $\omega > 0$ grow in an unstable manner, while the region $\omega < 0$ corresponds to a stable regime.

where $l = 2C/v$ is the diffusion length with C being the diffusion constant. Because of the above form for $\delta(x,t)$, ω represents the amplification rate of the perturbation, and its sign determines stability. For $\omega > 0$ the perturbations grow exponentially in time (instability), while they quickly die out if $\omega < 0$. Fig. 9.2 schematically shows the behaviour of ω as a function of the wave number k. It can be seen from this figure that in a region between $k = 0$ and $k_{max} = \sqrt{ld_0}$ the amplification rate is positive. The upper cutoff is due to the surface tension represented by d_0. If $d_0 = 0$, the growth rate increases indefinitely also for arbitrarily short wavelengths, and the problem is ill-posed from the physical point of view. The fastest growth occurs for

$$\lambda_c = 2\pi/k_c = \sqrt{3ld_0} \tag{9.6}$$

which is expected to be close to the characteristic wavelength of the pattern emerging from the competition of the stabilizing effect of the surface tension and the destabilizing effect of the Mullins-Sekerka instability. The capillary length d_0 is a microscopic quantity, typically of the order of Ångstroms. However, the diffusion length l is usually macroscopic, varying in a wide

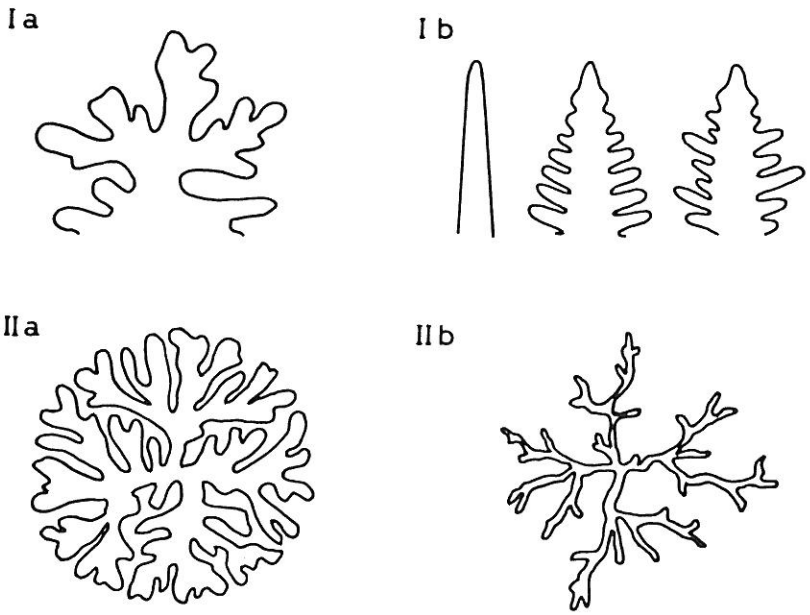

Figure 9.3. Schematic pictures of the major types of patterns which typically occur during unstable interfacial growth.

range depending on the given growth process. Thus, Laplacian growth may take place on very different length scales.

It is the unstable, non-linear nature of Eqs. (9.1-9.4) which is behind the sensitive dependence of the solutions on a number of factors influencing the growth of interfaces. Correspondingly, there exists a great variety of possible patterns which can be classified based upon their growth mechanism and geometrical properties (Vicsek 1987, Vicsek and Kertész 1988). Schematic drawings of the *major types of patterns* are shown in Fig. 9.3. In the first set the patterns are divided into two groups depending on the stability of the most advanced parts of the interface, called tips. Pictures Ia and Ib are intended to demonstrate that a tip can be either unstable and go through repeated tip splittings, or stable, and lead to dendritic growth. Unstable tips result in disordered structures with no apparent symmetry. If the tips are stable, in the sense that small perturbations around their stationary shape decay relatively quickly, the obtained patterns have a symmetry of varying degree. Picture Ib shows the three most commonly occurring possibilities.

In the other set (IIa and IIb) it is the geometry of the overall pattern which is qualitatively different for the two types of structures. In some

cases the interface bounds a region which is homogeneous on a length scale comparable to the size of the object, while under different conditions the growing pattern has an open branching structure and a corresponding fractal dimension. According to our present understanding all combinations of the above two sets occur in nature.

On the basis of the above discussion it is natural to raise the following questions:
i) What are the relevant parameters determining whether a given growth process leads to a fractal or to another type of complex pattern?
ii) What are the conditions under which a given parameter has a dominating effect on the shape of the interface?
In Part III we shall concentrate on describing numerical and experimental works aimed at answering these questions.

Experience with pattern forming systems indicated that anisotropy, randomness and driving force $(u_\Gamma - u_\infty)$ can play an essential role during unstable interfacial growth. Fortunately, computer simulations and model experiments allow the investigaton of the effects of these parameters on the formation of complex patterns. Of course, the question whether the Laplace equation with no noise and no anisotropy leads to fractal patterns represents one of the most interesting problems. However, at this point the interested reader will be disappointed: there exists no definite answer to this question yet.

9.2. MODELS RELATED TO DIFFUSION-LIMITED AGGREGATION

Aggregation models represent a recent approach to the problem of pattern formation. When using this method, the structure develops on a regular lattice as individual particles are added to a growing cluster. Simulating aggregation is an alternative to the more accurate numerical techniques (Section 9.4.) which are based on digitizing along the interface only. Because of this simplification some of the fine details are lost, however, using aggregation models more complex structures can be studied and the fluctuations enter the calculations in a natural way.

Many of the methods related to cluster growth are based on the diffusion-limited aggregation (DLA) model (Chapter 6.). It can be easily shown that DLA clusters and the solutions of Eqs. (9.1-9.4) should be closely connected (Witten and Sander 1983). Let $u(\vec{x},t)$ be the probability that a randomly walking particle released far from the interface will be at point $\vec{x}$ after having made t steps on the lattice. The probability of finding the particle at $\vec{x}$ equals the average of probabilities of finding it at the neighbouring sites at the previous time step

$$u(\vec{x},t+1) = \frac{1}{z}\sum_{\vec{a}} u(\vec{x}+\vec{a},t), \tag{9.7}$$

where $\vec{a}$ runs over the z neighbours of site $\vec{x}$. Deducting a term $u(\vec{x},t)$ from both sides of (9.7) we see that it represents the discrete version of the diffusion equation $\partial u/\partial t = C\nabla^2 u$. Since in DLA the particles are released one by one the changes in time are slow and we recover the Laplace equation (9.1). The probability that the perimeter site $\vec{x}$ gains a particle at time $t+1$ can be expressed analogously to (9.2)

$$v_n(\vec{x},t+1) = \frac{1}{z}\sum_{\vec{a}} u(\vec{x}+\vec{a},t). \tag{9.8}$$

Here v_n was used to express the fact that the velocity of the interface is given by the probability of gaining a particle at $\vec{x}$. Furthermore, the right-hand side of (9.8) corresponds to the gradient of u, because $u = 0$ at the sites adjacent to the growing cluster. In this way (9.8) is equivalent to the discretized version of the boundary condition (9.2). It should be pointed out that the above relations are true for the probability distribution, and in an actual simulation a single diffusing particle may visit sites with a frequency quite different from that predicted by the average behaviour. Finally, (9.3) is fulfilled by providing a steady flux of the particles released from distant points.

However, the boundary condition (9.4) is not satisfied in DLA. Instead of being a smooth function of the local curvature, the value of u at the surface is equal to zero, as was mentioned above ($d_0 = 0$ because the surface tension

is assumed to be zero. On the other hand, the lattice constant introduces a lower typical length scale, a property charcteristic for interfaces with non-zero surface tension). In fact, there exists no well defined interface curvature for diffusion-limited aggregation clusters: Fig. 6.1 shows that the typical curvature is trivially given by the lattice constant, or it is equal to zero. This is the first problem which has to be treated by the aggregation models constructed to simulate pattern formation. In addition, the structure of DLA clusters is largely determined by the fluctuations represented by the individual random walks of the incoming particles. To simulate experimental situations with varying degree of randomness one has to be able to control the amount of fluctuations present in the aggregation process. The algorithms resolving these problems will be described in the next two Subsections.

9.2.1. Effects of surface tension

To solve the Laplace equation it is sufficient to determine the value of the field u at the boundary of the two phases. Then the solution can be written as the sum over the geometry dependent Green's function $G(\vec{x},\vec{s})$ weighted by the boundary value $u_\Gamma(\vec{s})$

$$u(\vec{x}) = \sum_{\vec{s}\in\Gamma} G(\vec{x},\vec{s}) u_\Gamma(\vec{s}), \tag{9.9}$$

where the summation runs over all points on the interface and $G(\vec{x},\vec{s})$ is the electric field generated by a point charge source located at $\vec{s}$ on a grounded conductor.

It can be shown that $G(\vec{x},\vec{s})$ is proportional to the probability that a random walk starting from $\vec{s}$ visits $\vec{x}$ before hitting the interface again (Kadanoff 1985, Szép *et al* 1985). This quantity can be estimated by counting the number of times the point $\vec{x}$ is visited by random walkers which are released from the surface point $\vec{s}$ and terminate whenever they hit any occupied site. Thus we need two types of walks: i) particles released far from the interface represent the constant boundary condition $u_\infty = Const$ (9.3). ii) The second type of walks leave the surface point $\vec{s}$ with a probability

$u_\Gamma(\vec{s}) = d_0\kappa$ corresponding to the boundary condition (9.4), and end at another surface point. These walks transfer flux from one part of the interface to the other, changing its shape.

During the simulations (Kadanoff 1985, Szép *et al* 1985, Liang 1986) one first determines the bonds connecting the surface sites of the growing cluster with their nearest neigbouring empty sites. The total number n_t of net crossings of random walkers through these bonds is recorded (adding to n_t 1 for incoming and deducting from n_t 1 for departing particles). Then the interface is moved forward if n_t reaches a previously fixed number m and moved backward if n_t becomes smaller than $-m$. Here m controls the fluctuations: for $m \gg 1$ the noise due to the randomness of the walks is almost averaged out (see next section). There is a practical difficulty in using (9.4) for the determination of the probability of releasing a particle from a surface point since κ can have both positive and negative values, while the probability $u_\Gamma(\vec{s})$ has to be always positive. This problem is resolved by letting the particles carry a "flux" f and using, instead of (9.4),

$$f u_\Gamma(\vec{s}) = d_0\kappa \tag{9.10}$$

and let κ and f have the same sign ($f = 1$ or $f = -1$).

There are several possibilities for the estimation of the surface curvature κ at site $\vec{s}$. A simple procedure is based on counting the number of particles, N_L, belonging to the aggregate and being within a distance L from $\vec{s}$ (Vicsek 1984). Assuming that the characteristic changes in the shape of the surface occur on a scale larger than L, for example, the quantity

$$\kappa = \frac{3}{L}\left(\frac{N_L}{L^2} + \frac{\pi}{2}\right) \tag{9.11}$$

provides a reasonable estimate for κ on a square lattice.

The above method can be used to simulate pattern formation under various conditions. Fig. 9.4 demonstrates that it leads to patterns (Liang 1986) matching the experimental results obtained in the studies of viscous

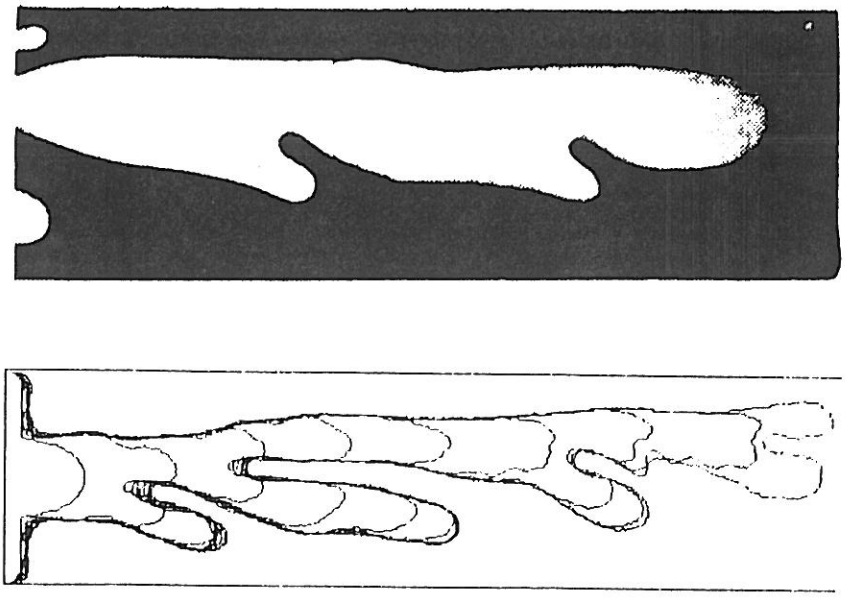

Figure 9.4. Experimental (upper picture, Park and Homsy 1985) and simulated (Liang 1986) viscous fingers obtained in the longitudinal geometry.

fingering in a longitudinal Hele-Shaw cell (air injected into glycerin placed between two close parallel glass plates). Very different shapes can be generated by changing m and the ration of the number of walkers released from the interface and far from it. For large m the generated structures resemble dendritic growth (Szép *et al* 1985).

Pattern formation in diffusion-limited aggregation can be studied by a considerably simpler model as well. Perhaps the easiest way to take into account the effects of surface tension is to introduce a sticking probability $p_s(\kappa)$ depending on the local surface curvature (Vicsek 1984). A plausible choice is

$$p_s(\kappa) = A\kappa + B, \tag{9.12}$$

where A and B are constants. The analogy with the boundary condition (9.4) is provided by the fact that the sticking probability is proportional to the local growth velocity. If p_s calculated from (9.12) is less than 0 it is set to a

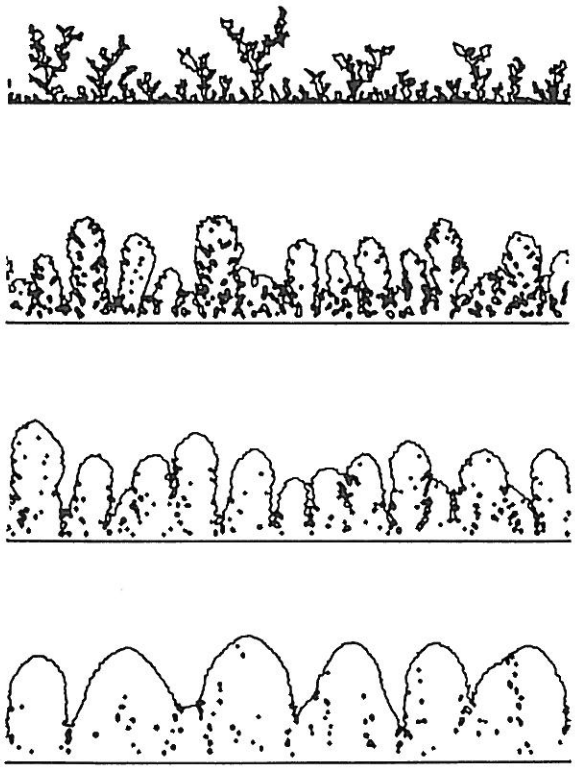

Figure 9.5. Interface of the diffusion-limited deposits with curvature-dependent sticking probability and relaxation. The following values were used for the parameters in Eq. (9.12): (a) A=0, B=1; (b) A=3, B=0.5; (c) A=6, B=0.5 and (d) A=12, B=0.5 (Vicsek 1984).

small threshold value, and if $p_s > 1$, it is assumed to be equal to 1. For short times there is a direct correspondence between this method and the algorithm described at the beginning of this Section (Sarkar 1985). The analogy can be understood on a qualitative basis: A particle which does not stick to the surface can be regarded as starting a walk from the given point of the interface. In the present model one has to use an additional rule to obtain well defined surfaces. According to this rule a particle previously allowed to stick is relaxed to its final position which is one of the nearest neighbour sites with the largest number of nearest neighbours (with the lowest potential energy).

This curvature dependent sticking probability model can be used to demonstrate the role of surface tension in the development of diffusion-limited patterns in the presence of noise. Fig. 9.5 shows a series of simulations

carried out in the strip geometry with an increasing value of the parameter A corresponding to the surface tension. These pictures illustrate that for a fixed size of the system there is a crossover from a fractal-type structure to a less disordered, quasi-regular geometry. Although not shown in Fig. 9.5, it has to be noted that none of the structures is stable, and for longer "times" (more particles added) the competition among the fingers results in patterns similar to either Fig.9.5a or to a single finger (the latter is observed for larger A).

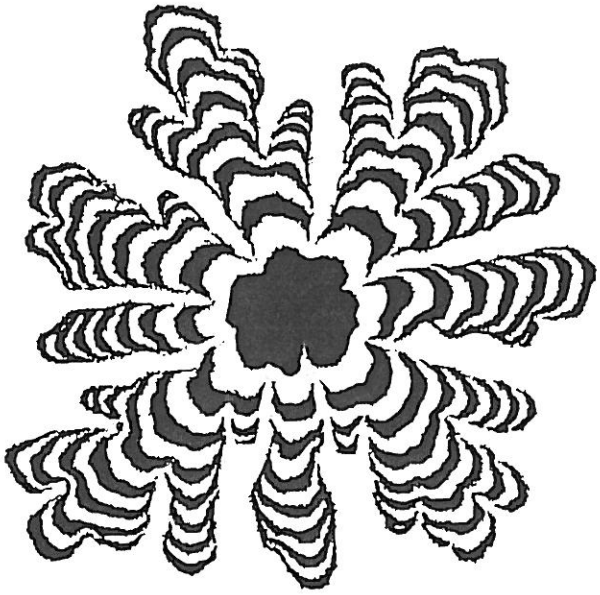

Figure 9.6. Various stages in the growth of an off-lattice cluster generated using a curvature-dependent sticking probability. This figure illustrates the crossover from a compact to a fractal structure as the aggregate grows larger (Meakin *et al* 1987).

The patterns displayed in Fig. 9.5 were generated on a square lattice whose anisotropy is known to affect the results when aggregation on a single seed particle is simulated. To study *viscous fingering* in the radial Hele-Shaw cell (Section 10.1.1.) under *isotropic* conditions one has to use the off-lattice version of DLA with a sticking probability given by (9.12) (Meakin *et al* 1987). A typical pattern generated using this approach is displayed in Fig. 9.6, where the black and white layers indicate the successive stages of the growth. The initially circular shape becomes unstable when its radius exceeds the radius of curvature characteristic for the given value of A. In DLA tip

splitting occurs as a one time event due to the microscopic fluctuations only, while in Fig. 9.6 the growing tips seem to split gradually.

On the basis of Figs. 9.5 and 9.6 we conclude that for a fixed system size, decreasing the surface tension leads to structures with a more pronounced fractal behaviour. This is in agreement with the experimental observation of fractal viscous fingers in a system with zero interfacial tension (Daccord *et al* 1986). One possible explanation is that noise plays an increasingly relevant role as the surface tension is decreased. Similarly, in Fig. 9.5 a crossover from a quasi-regular to a disordered pattern can be seen as a function of the size of the aggregates. Thus, these simulations suggest that in the presence of noise (even if it is small) the asymptotic shape of Laplacian patterns growing out from a centre has a fractal structure presumably analogous to that of DLA (Vicsek 1985, Meakin *et al* 1987).

9.2.2. Noise reduction in DLA

We have seen above that the surface tension does not change the asymptotic behaviour of patterns if i) the simulations are carried out off-lattice (isotropy), and ii) the fluctuations can not be neglected. In this Section we shall concentrate on the *interplay of anisotropy and noise* during the growth of complex diffusion-limited patterns. This problem can be investigated by the noise reduced version of on-lattice DLA described below (Tang 1985, Szép *et al* 1985, Kertész and Vicsek 1986). For simplicity, we shall not treat the effects of surface tension in the form discussed in the previous section since the finite size of the particles can be regarded as representing a small finite surface tension.

There is a natural way to decrease the fluctuations in DLA (Kertèsz and Vicsek 1986). Instead of adding a particle to the aggregate immediately after it hits a growth site, one keeps a record of how many times each of the perimeter sites (empty sites adjacent to the cluster) becomes a termination point for a randomly walking particle. After a perimeter site has been contacted m times it is filled and the new perimeter sites are identified. The scores (number of contacts) associated with these sites are set to zero. The

scores associated with all of the other surface sites remain at their values before this event. Clearly, this procedure decreases the noise with growing m, because probing the surface with many walks provides a better estimate of the expectation value of the growth rate at the given point than a single walk. In the limit $m \to \infty$, application of the method yields the solution of the lattice version of the noiseless Laplace equation (9.1) with the boundary conditions (9.2) and (9.3).

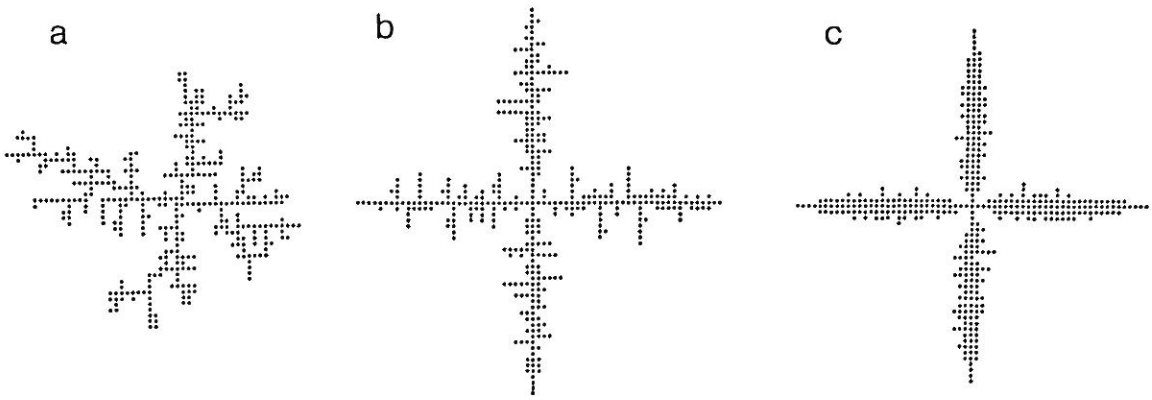

Figure 9.7. Clusters consisting of 400 particles generated on the square lattice using the noise-reduced diffusion-limited aggregation algorithm. (a) m=2, random fractal; (b) m=20, dendritic growth, and (c) m=400, noisy needle crystal (Kertész and Vicsek 1986).

Fig. 9.7 shows three representative clusters generated on a square lattice with various values of the noise reduction parameter m. The overall appearance of the aggregates indicates that as a function of decreasing noise (increasing m) two types of morphological changes occur in these small scale simulations. At about $m = 5$ the random, tip-splitting structure typical for DLA clusters crosses over into a dendritic pattern with well defined but irregularly spaced side branches having stable tips. Further increasing m results in the growth of a structure consisting of four needles growing out from the centre along the lattice axes.

The above described morphological changes taking place in the sequence *random fractal* $\to$ *dendritic* $\to$ *needle* are results of the competition between the anisotropy provided by the underlying square lattice and the

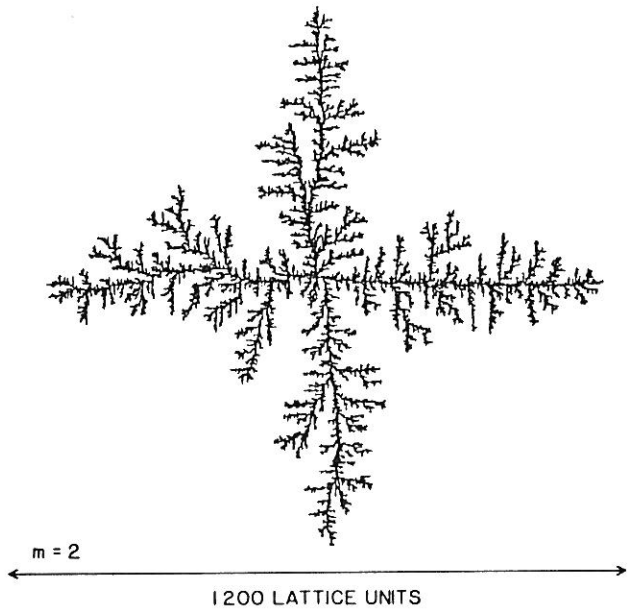

Figure 9.8. Noise-reduced diffusion-limited aggregate (m=2, N=50,000) generated on the square lattice (Kertész *et al* 1986).

fluctuations due to the random walks. An analogous result is obtained for fixed m and increasing cluster size (Kertész *et al* 1986). Fig.9.8 shows that aggregates with $m = 2$ have asymptotically a cross-like shape, while for much smaller sizes their envelope is approximately circular. As was discussed in Section 6.1.2. the overall shape of extremely large diffusion-limited aggregates grown on a square lattice is approaching a cross. Thus, the method of noise reduction seems to reveal the *asymptotic behaviour* of DLA clusters using considerably smaller number of particles. In conclusion, in a far-from-equilibrium growth process the structure of the interface can change non-trivially as a *function of size.* In the present case this is due to the fact that on a long run lattice anisotropy dominates over the disorder due to fluctuations.

The clusters generated on lattices using noise reduced DLA are expected to reflect some of the relevant features of large Laplacian patterns with anisotropic surface tension growing in the presence of fluctuations. These aggregates usually have the overall shape of a $2n$-fold star, where n is the number of axes of the underlying lattice. A convenient approach to the characterization of such clusters is to define two exponents $\nu_{||}$ and $\nu_{\perp}$ through

the expressions (6.13) and (6.14) describing respectively the scaling of the average length l and width w of the arms of the clusters as a function of the number of particles in them. Large scale simulations for $m > 1$ indicate that in the asymptotic limit both exponents are somewhat larger, but close to $\nu_{||} \simeq \nu_{\perp} \simeq 2/3$ (Meakin 1987). Correspondingly, the fractal dimension of the noise-reduced DLA clusters is about $D \simeq 1.5$.

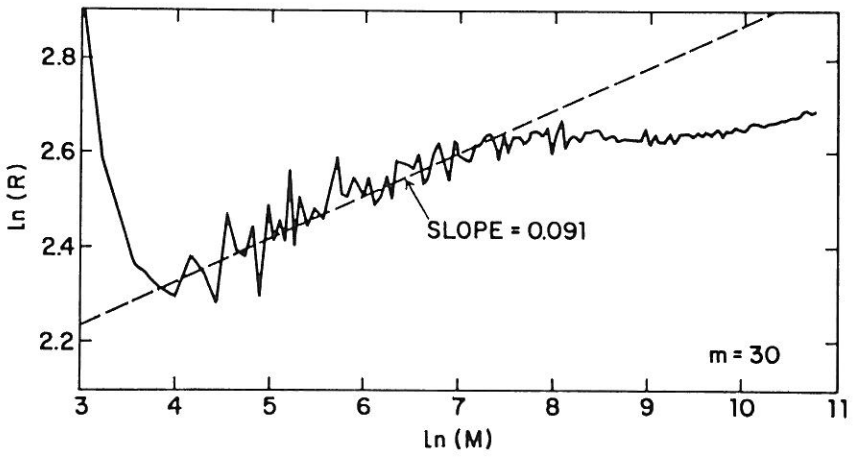

Figure 9.9. Dependence of the ratio l/w on the size of the aggregates grown on the square lattice with a noise reduction parameter $m = 30$. l and w denote respectively the length and the width of the main arms of the clusters (Meakin 1987).

The situation is quite delicate, as is illustrated by Fig. 9.9, where the logarithm of the ratio $R = l/w$ is plotted versus the logarithm of the number of particles, N, in the clusters. For intermediate cluster sizes the data show scaling of R with N of the form $R \sim N^{\nu_{||} - \nu_{\perp}}$, and the $R \simeq Const$ behaviour is manifested only above a certain size. This result suggest that $\nu_{||} > \nu_{\perp}$ obtained for very large ordinary diffusion-limited aggregates is not necessarily valid in the asymptotic limit (it describes a transient situation).

9.3. GENERALIZATIONS OF THE DIELECTRIC BREAKDOWN MODEL

In its simplest form the dielectric breakdown model (DBM) discussed in Section 6.3. exhibits a fractal scaling analogous to that of DLA. However,

various modifications of DBM result in qualitative deviations between the two models. We briefly recall that in DBM the Laplace equation is solved on a lattice to obtain the growth probabilities associated with the perimeter sites, instead of releasing random walkers as is done in DLA. Then a perimeter site is filled with a probability proportional to some power (η) of the calculated growth probability. This procedure makes the method quite versatile, e.g., it can be used to grow deterministic patterns as well (Section 6.4.). Furthermore, it has a parameter η which provides an additional opportunity to generate a family of qualitatively different patterns corresponding to a non-linear dependence of the growth velocity on the local gradient.

There is a difference between the boundary conditions which are used when DLA and DBM clusters are generated. The condition that a randomly walking particle sticks to the aggregate when it arrives at a site adjacent to the cluster (DLA) is equivalent to keeping the probability equal to zero at the *perimeter* sites. In the case of DBM one sets the field equal to zero on the *surface* sites (sites already filled). This seemingly small difference becomes relevant when noise-reduced versions of DLA and DBM are considered. To decrease the fluctuations in DBM one fills a new perimeter site only after it has been chosen m times. Again, $m \to \infty$ corresponds to deterministic growth.

Application of the above method with $m = 20$ on the triangular lattice (Nittmann and Stanley 1986) results in tip splitting patterns very similar to that shown in Fig. 9.6. On the other hand, noise-reduced DLA clusters on the same lattice have stable tips, and look like random snowflakes since they are sixfold analogues of the patterns displayed in Fig. 9.7. Obviously, DBM is less susceptible to lattice anisotropy than DLA. It has to be emphasized that using DBM with $m > 1$ one obtains disordered structures with branches having a well defined, m-dependent thickness, without taking into account the surface tension. Although this finding is somewhat surprising, a similar behaviour is found in the experiments on viscous fingering with miscible fluids, where interfaces with characteristic curvatures can be observed (Paterson 1985). Thus the noise-reduced DBM may offer help to understand some of the properties of moving interfaces with zero surface tension.

Figs. 9.4-9.7 demonstrate that aggregation models can be useful in studying the growth of realistic geometrical structures of various kinds, including viscous fingers. One of the most appealing challenges is, however, to understand the development of such intricate objects as snowflakes and other related dendritic crystals. In the remaining part of this section we shall concentrate on models producing patterns relevant to the growth of complex dendritic structures.

Snowflakes exhibit a number of very characteristic features. They (a) are quasi two-dimensional, (b) have sixfold symmetry and (c) can have a large number of entirely different shapes. To grow snow crystals in the computer one can use variations of the DBM on the triangular lattice, which provides the two-dimensional nature and the sixfold symmetry of the patterns simultaneously. Thus the properties (a) and (b) are built into the simulations by this restriction. However, at this point our goal is not to explain (a) or the fact that snowflakes have six arms (these properties are due to the anisotropy of the surface tension). Instead, we shall be more concerned with the statement (c).

Fig. 9.10 shows patterns which are quite similar to the real snowflakes also displayed in the figure. The simulated clusters were obtained using the following model (Nittmann and Stanley 1987). i) The growth probability is determined by solving the Laplace equation on the triangular lattice with a boundary condition corresponding to DLA, i.e., setting the field u equal to zero at the perimeter sites. ii) Perimeter sites are picked randomly, with a probability proportional to $(\nabla u)^\eta$. iii) A perimeter site is filled if it has been chosen m times. As the non-linearity parameter η is increased, qualitatively different patterns are obtained. Although there exists no direct physical interpretation of the parameter η, one expects that the complicated processes taking place on the surface of a snowflake may give rise to a non-linear response to the local gradient of the field (temperature). In addition, one can simulate the effects of surface tension which leads to the thickening of arms and the disappearance of small holes.

Since snowflakes are *almost perfectly symmetric*, one expects that they can be studied effectively by *deterministic growth models* (Section 6.4.). It is

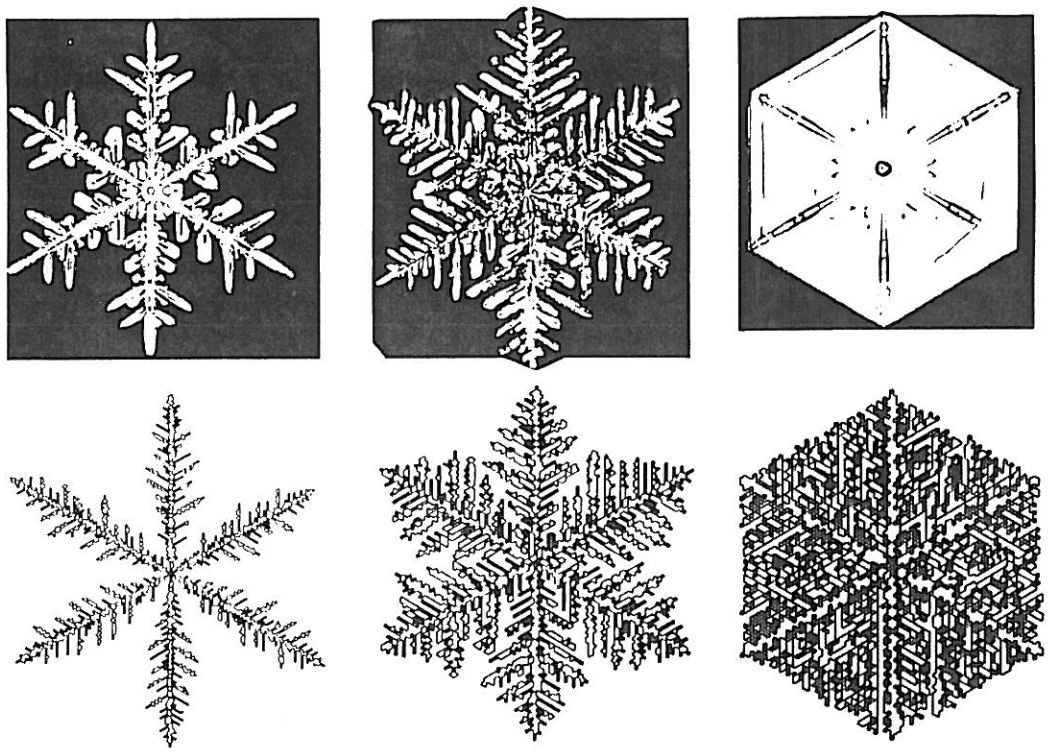

Figure 9.10. Real (top row, reproduced from Bentley and Humpreys (1962)) and simulated (bottom row) snowflakes. The simulated patterns were generated on the triangular lattice up to 4000 particles with $m = 200$. The value of the exponent η for patterns (a-c) was equal to 0.05, 0.5 and 1.0 (Nittmann and Stanley 1987).

natural to assume that the low level of randomness in the shape of snowflakes is due to the fact that the fluctuations in the conditions affecting the growth process take place on a length scale larger than the size of a snowflake. To simulate the development of dendritic patterns with the spatial fluctuations neglected, the following method can be used.

The process starts with a seed particle placed on a triangular lattice. At each time step the value of the field u is calculated by solving the lattice version of the Laplace equation (9.1). The value of the field is assumed to be zero on a circle having a radius a couple of times larger than the size of the cluster. For the surface sites u is prescribed by (9.4), in which κ is calculated by a method described in the previous Section and the kinetic term is neglected. The gradients at the surface are normalized onto the unit

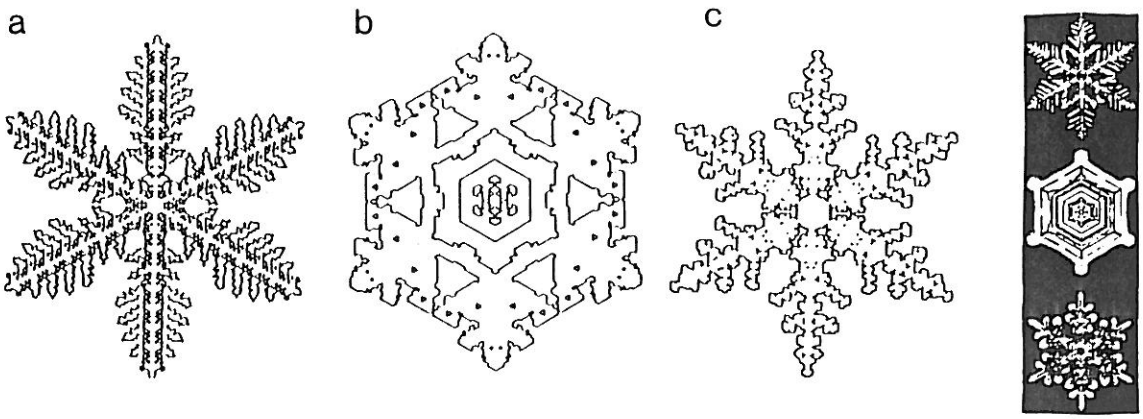

Figure 9.11. Three examples for patterns generated by the deterministic growth model on a triangular lattice. (b) and (c) were obtained by changing the parameters a and b of equation (9.13) randomly during the growth (Family *et al* 1987). The inset shows a few typical snowflakes reproduced from Bentley and Humpreys (1962).

interval and those perimeter sites for which the gradient is larger than q are filled.

To approximate the boundary condition (9.2) one assumes that q varies in time as (Family *et al* 1987)

$$q(t) = a + b(t \bmod [c]) \tag{9.13}$$

which is a piecewise function depending on the parameters a, b and c. This expression ensures that the growth velocity is proportional to the local gradient in a discretized manner (if the local gradient is small, its value exceeds $q(t)$ less frequently and this results in a slower growth). By varying a and b the effects caused by surface diffusion and changing undercooling can be simulated.

The above method is capable of producing most of the symmetric patterns observed in the related experiments. The various cases include faceted growth and structures corresponding to needle and fractal crystals. If the parameter a is changing in time, the combinations of these patterns

are obtained within a single cluster. In Fig. 9.11 a few examples are shown, where the sixfold symmetry is provided by the underlying triangular lattice. There is a striking similarity between the simulated and the real snowflakes (also displayed).

Perhaps the most important conclusion which can be drawn from the study of the above methods is related to the seemingly unlimited number of symmetric structures produced in dendritic growth. These models demonstrate that the great variety of patterns appearing as a result of the same solidification process is likely to be induced by the *temporal changes* in the environmental conditions during crystallization. Indeed, snowflakes fall through regions of air with more or less randomly changing temperature and vapour pressure, and it is the time dependent interplay of such factors as undercooling, surface tension and surface diffusion which leads to the observed rich behaviour.

9.4. BOUNDARY INTEGRAL METHODS

Simulation techniques involving aggregation of particles are bound to describe the behaviour of the discrete version of the Laplace equation. Correspondingly, the obtained patterns are either influenced by the fluctuations present in the algorithms or are determined by the lattice anisotropy. However, in many experimental situations (for example in viscous fingering) the motion of the interface is expected to be described by the continuum version of (9.1) without any significant amount of external noise.

The complex interfacial patterns in such cases seem to emerge as a result of the initial surface geometry and the subsequent proliferation of tip-splitting instabilities. This observation suggests an analogy with deterministic chaos: slightly different initial configurations may lead to very different disordered patterns because the instabilities amplify the smallest deviations.

To study this aspect of fractal pattern formation one is led to solving the Laplace equation without using an underlying lattice. This can be achieved by the so called *boundary integral method* in which for $d = 2$ the

free interface is approximated as a piecewise linear with uniform monopole sources along each leg. A given interface uniquely determines the source distribution which, in turn, uniquely determines the velocity distribution along the interface.

The above idea is based on converting Eqs. (9.1-9.4) to an integro-differential equation (Kessler *et al* 1984, Gregoria and Schwartz 1986). Before doing so, for convenience we confine ourselves to the two-dimensional case and replace the boundary condition (9.3) and (9.4) with the essentially equivalent conditions $u(R_0) = 0$ and $u_\Gamma = 1 - \kappa(\vec{x}_s)$, where R_0 is the radius of a circle much larger than the growing object and the kinetic term in (9.4) is neglected. Furthermore, using the language of solidification, we can say that the boundary condition (9.2) corresponds to the fact that an element of the interface at position $\vec{x}_s$ represents a source of temperature of an amount proportional to $v_n(\vec{x}_s)$. Then the temperature at any other point is the background temperature (which is now assumed to be equal to zero) plus the superposition of sources at all interface points propagated by the diffusion Green's function. Therefore,

$$u(\vec{x}) = \int dx'_s G(\vec{x}, \vec{x}'_s) v_n(\vec{x}'_s), \tag{9.14}$$

where the Green's function for the two-dimensional Laplace equation is

$$G(\vec{x}, \vec{y}) = \ln(\vec{x} - \vec{y})^2 + \ln(R_0^2 \vec{y}/y^2 - \vec{x})^2 - \ln(R_0/y^2). \tag{9.15}$$

The equivalence of (9.14) to (9.1) and (9.2) can be shown by noting that for points not belonging to the interface the Laplace equation is satisfied, because

$$\nabla^2 G(\vec{x}, \vec{y}) = -\delta(\vec{x} - \vec{y}), \tag{9.16}$$

where $\delta(\vec{x})$ denotes the Dirac delta function. The boundary condition (9.2) is also satisfied since

$$-c\frac{\partial u}{\partial n}|_\Gamma = -\int\int \frac{\partial G}{\partial n}|_\Gamma \cdot v_n(\vec{x}') = v_n(\vec{x}). \tag{9.17}$$

The above expression is based on a standard result of potential theory which can be obtained using Green's theorem. According to this result the discontinuity in the normal derivative of G is a delta function. The final equation is obtained by calculating u at the interface and satisfying the boundary condition $u_\Gamma = 1 - \kappa(\vec{x}_s)$. The result is

$$1 + c\int dx'_s \kappa(\vec{x}_s)\frac{\partial}{\partial n'}G(\vec{x}_s, \vec{x}'_s) = \int dx'_s G(\vec{x}_s, \vec{x}'_s)v_n(\vec{x}'_s), \tag{9.18}$$

where the integral on the left-hand side is the potential due to a dipole layer of strength $-c\kappa$, which provides a discontinuous jump in the field from 1 in the interior to $1 - \kappa$ on the interface.

Next one parametrizes the interface by using the variables $\theta(s)$ and s_T, where $\theta(s)$ is the angle between the normal to the curve and a fixed direction in space, and s_T is the total arc length. The angle $\theta(s)$ is defined as a function of the distance (arc length) s along the interface. The equations of motion for these quantities are (Kessler *et al* 1984)

$$\partial\theta(s)/\partial t = -\partial v_n/\partial s \tag{9.19}$$

$$\partial s_T/\partial t = \int_0^{s_T} ds\kappa(s)v_n(s). \tag{9.20}$$

The following procedure is used to determine the development of the interface. At any fixed time the discretized $\theta(s_i)$ is given, thus we can construct the curve $\vec{x}_{s_i}$ by quadrature. The integral equation (9.18) is rewritten as a discrete matrix equation for $v_n(\vec{x}_{s_i})$. After having solved the corresponding system of linear algebraic equation for $v_n(\vec{x}_{s_i})$, (9.19) and (9.20) are used to step the interface forward in time using a predictor-corrector method.

The main limitation of the above procedure is represented by the number of grid points M required for discretizing the arc length. There is a

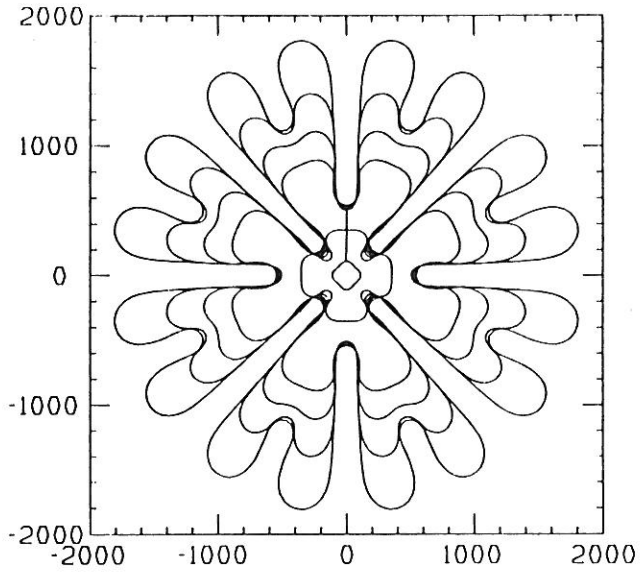

Figure 9.12. Snapshots of the interface growing out from a fourfold seed. This figure was obtained by the boundary integral method. The axes are in the units of the capillary length (Sander *et al* 1985).

condition depending on the surface tension which sets an upper limit for distance between the grid points, thus M increases with the total arc length. Since M is the number of columns of the matrix to be set up in Eq. (9.18), in a medium-scale calculation with a fourfold symmetric object (Sander *et al* 1985) one reaches the computational limit when M is about 4000. Fig. 9.12 shows a typical interface at this limit demonstrating the difficulty of obtaining a structure close to the complexity of a DLA type fractal pattern using the boundary integral approach. Furthermore, the displayed pattern seems to be space filling rather than becoming increasingly sparse (the latter property would indicate the fractal nature of the interface).

The boundary integral method is particularly suitable for the investigation of the effects caused by a small amount of controllable *anisotropy* (Kessler *et al* 1984). Let us assume that the angular dependence of the surface tension in the boundary condition (9.4) is of the form

$$u_\Gamma = -d_0[1 + \epsilon\cos(n\theta)]\kappa, \tag{9.21}$$

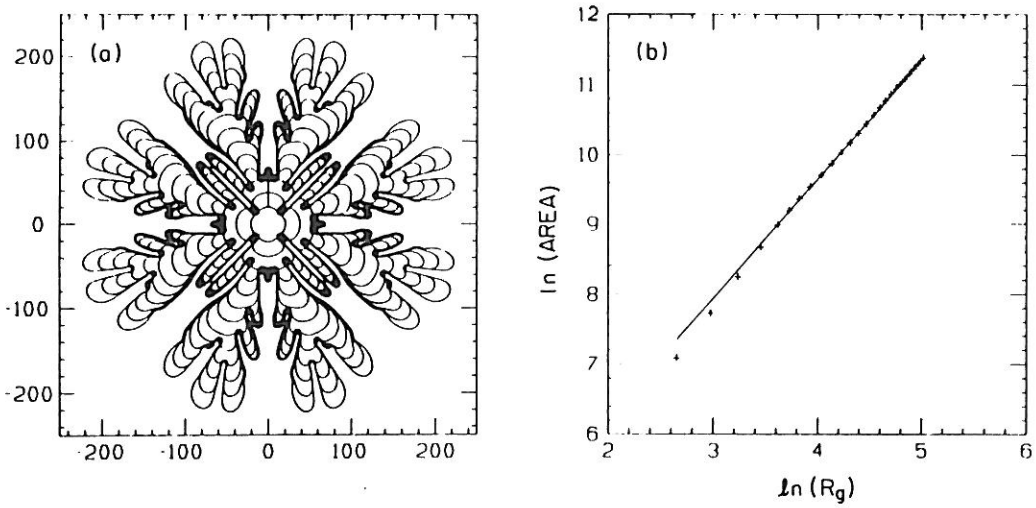

Figure 9.13. (a) Growth of a fourfold interface obtained for $K = 5$. (b) From the scaling of the area of the pattern in Fig. 13a with its radius the estimate $D \simeq 1.72$ can be obtained for the effective fractal dimension (Sander *et al* 1985).

where ϵ is a small parameter and $n = 4$ for a pattern with four preferred growth directions. According to the numerical simulations with various ϵ, the anisotropy of the surface tension has to be larger than a well defined threshold value (close to 0.1 for $n = 4$) in order to give rise to dendritic growth with stable tips. However, the calculated patterns are again of relatively simple structure because of the above mentioned computational limitations.

One possibility to obtain more complex interfaces is to change the curvature dependence in the boundary condition (9.4) arbitrarily to κ^K, where K is an odd positive integer (Sander *et al* 1985). Obviously, for large K small curvatures have no effect, which corresponds to an effective decrease of the surface tension. Consequently, the typical curvature increases to a K-dependent value, and more complex patterns using the same number of grid points can be obtained. The zero surface tension limit can be simulated by $K \to \infty$. In the diffusion-limited aggregation model there is no surface tension except for an upper cutoff for the surface curvature provided by the lattice spacing. A calculation with $K \gg 1$ is expected to simulate the deterministic version of DLA, but it should be noted that the real physical growth is determined by the boundary condition with $K = 1$.

Fig. 9.13a shows a representative pattern obtained for $K = 5$. (In these calculations the term $\kappa(\vec{x}_s)$ in (9.18) has to be replaced with $\kappa^K(\vec{x}_s)$.) The fractal dimension of the object bounded by the interface can be estimated by determining the scaling of its area with its radius of gyration R_g. The resulting plot (Fig. 9.13b) suggests that one can associate a fractal dimension $D \simeq 1.72$ with the object shown in Fig 9.13a, although it does not possess a high degree of complexity.

As we have seen, the boundary integral method directly provides a set of velocities $v_n(\vec{x}_{s_j}) = v_j$ corresponding to the motion of the j-th grid point on the interface. Let us introduce $p_j = v_j / \sum_j v_j$, the set of normalized velocities, which has a relation to the growth probability measure defined e.g. for DLA. Obviously, the local velocity of the interface determines the distance by which the interface advances during the next time step, and this distance is linearly proportional to the growth probability in a cluster growth model (both are given by the gradient of the associated fields). This analogy can be used to compare the *multifractal* properties of DLA clusters and the continuous interfaces generated by the boundary integral method with a boundary condition similar to (9.4), but depending on the surface curvature according to κ^K (Ramanlal and Sander 1987). Defining $p_i(\epsilon)$ as the average normalized velocity in the i-th region of size ϵ one can use the formalism described in Chapter 3. to calculate the spectrum of fractal dimensionalities $f(\alpha)$.

To determine $f(\alpha)$, the generalized fractal dimensions D_q are evaluated numerically for the final stage of growth in Fig. 9.13a, by plotting $\ln \sum p_i^q(\epsilon)$ as a function of $\ln \epsilon$ and measuring the slope in the region $16 < \epsilon < 100$. The functions α_q, f_q and $f(\alpha)$ are subsequently calculated using (3.11) and (3.13-3.15).

The result for $f(\alpha)$ is shown in Fig. 9.14. It is in reasonable agreement with the multifractal spectrum obtained for DLA clusters (see Section 6.1.4.). (There is a region about the numerically singular point $q = 1$ where no data are given.) One can use two methods to subtract estimates from $f(\alpha)$ for the fractal dimension D. First, in a large system its maximum, f_{max}, is equal to D. In the present case $f_{max} \simeq 1.627$. Second, one obtains another value

for the fractal dimension from the relation (6.31) $D = 1 + \alpha_{min} \simeq 1.684$, where α_{min} is the smallest measured value of α. Since with growing size f_{max} is increasing while α_{min} is decreasing, one is led to the conclusion that the fractal dimension of the continuous interfaces used to simulate continuum DLA has to be in the range $1.627 < D < 1.684$. Further careful analysis of the results suggests a value close to 1.65. This estimate is different from $D \simeq 1.71$ obtained from large scale simulations of the diffusion-limited aggregation model. The relevance of this discrepancy is not clear because of the relatively small size of the investigated patterns.

In conclusion, investigations based on the boundary integral method demonstrate that i) noise is not a necessary ingredient of an algorithm producing DLA-type patterns since they can be grown using deterministic equations, ii) this result is supported by multifractal analysis and iii) the fractal dimension of off-lattice DLA clusters in the asymptotic limit may be approximately equal to 1.65. However, studies of larger systems are needed for making more definite statements.